Diversity of fate outcomes in cell pairs under lateral inhibition

Nara Guisoni[1,2,*], Rosa Martinez-Corral[1,*], Jordi Garcia Ojalvo[1,#], and Joaquín de Navascués[3,#]

[1] Department of Experimental and Health Sciences, Universitat Pompeu Fabra, Barcelona Biomedical Research Park (PRBB), Dr. Aiguader 88, 08003 Barcelona, Spain.

[2] Instituto de Física de Líquidos y Sistemas Biológicos, CONICET & Universidad Nacional de La Plata, Calle 59-789, 1900 La Plata, Argentina.

[3] European Cancer Stem Cell Research Institute, School of Biosciences, Cardiff University, Hadyn Ellis Building, Maindy Road, Cardiff CF24 4HQ, UK.

[*] Equal contribution

[#] Correspondence: denavascuesj@cardiff.ac.uk, jordi.g.ojalvo@upf.edu

Key words: Lateral inhibition, Notch-Delta signalling, symmetric cell division, intestinal stem cells, neutral competition

Summary statement: Notch/Delta-mediated lateral inhibition in cell pairs can result in symmetric signalling depending on the activation threshold, which can modulate cell-fate decisions depending on contact area.

Abstract

Cell fate determination by lateral inhibition via Notch/Delta signalling has been extensively studied. Most formalised models consider Notch/Delta interactions in fields of cells, with parameters that typically lead to symmetry breaking of signalling states between neighbouring cells, commonly resulting in salt-and-pepper fate patterns. Here we consider the case of signalling between isolated cell pairs, and find that the bifurcation properties of a standard mathematical model of lateral inhibition can lead to stable symmetric signalling states. We apply this model to the adult intestinal stem cell (ISC) of *Drosophila*, whose fate is stochastic but dependent on the Notch/Delta pathway. We observe a correlation between signalling state in cell pairs and their contact area. We interpret this behaviour in terms of the properties of our model in the presence of population variability in contact areas, which affects the effective signalling threshold of individual cells. Our results suggest that the dynamics of Notch/Delta signalling can contribute to explain stochasticity in stem cell fate decisions, and that the standard model for lateral inhibition can account for a wider range of developmental outcomes than previously considered.

2

Introduction

The Notch/Delta signalling pathway is one of the main regulators of cellular differentiation during development and adult tissue maintenance (reviewed in Artavanis-Tsakonas et al., 1999; Ehebauer et al., 2006; Koch et al., 2013). It often drives mutually inhibitory interactions between cells, acting as a gate for differentiation. This mode of action has been termed lateral inhibition, and has been the object of experimental study as well as mathematical formalisation for decades (see, for instance, Othmer and Scriven, 1971; Collier et al., 1996; Sprinzak et al., 2011; Petrovic et al., 2014). Quantitative models of lateral inhibition usually involve a field of cells expressing initially similar amounts of the receptor Notch and its membrane-bound ligand Delta. Delta trans-activates Notch in neighbouring cells and Notch, once activated, reduces in turn the ability of the cell to signal through Delta, leading to a state of mutual repression. This symmetry (and cell fate equivalence) is eventually broken by enforced biases and/or stochastic variation in Notch/Delta levels (Collier et al., 1996; Plahte, 2001; reviewed in Simpson, 2001) resulting in extended fine-grained spacing patterns (Othmer and Scriven, 1971; Collier et al., 1996; see also Shaya and Sprinzak, 2011) that have been experimentally characterized in depth in real developmental systems (reviewed in Greenwald, 1998; Arias and Stewart, 2002). In contrast, little attention has been paid so far to the effect of lateral inhibition in isolated cell pairs, beyond the trivial expectation that symmetry breaking will eventually take place, leading to cells taking opposing fates (see for instance, Collier et al., 1996; Rouault and Hakim, 2012). However there has been no formal investigation of whether alternative steady states are possible, perhaps due to the lack of an experimental model to relate it to.

The cellular homeostasis of the adult *Drosophila* midgut (Fig. 1A-D) can provide this experimental scenario, as in this tissue Notch/Delta signalling occurs mostly in isolated pairs of cells (Ohlstein and Spradling, 2006; de Navascués et al., 2012; Goulas et al., 2012). The fly's intestinal lining is maintained by intestinal stem cells (ISCs), which divide to both self-renew and

71 provide committed progenitors (Fig. 1B). Progenitors specialise in producing

72 either nutrient-absorbing enterocytes or secretory enteroendocrine cells (Guo

73 and Ohlstein, 2015; Micchelli and Perrimon, 2006; Ohlstein and Spradling,

74 2006; Zeng and Hou, 2015). The precursors of enterocytes, called

75 enteroblasts (EBs) are frequently found forming pairs with ISCs (Ohlstein and

76 Spradling, 2006; Micchelli and Perrimon, 2006; Bardin et al., 2010; de

77 Navascués et al., 2012) (Fig. 1C). These pairs are thought to result from an

78 earlier division of an ISC and subsequent fate allocation by Notch signalling,

79 before a new division or terminal differentiation event takes place (Goulas et

80 al., 2012; de Navascués et al., 2012). Importantly, ISC divisions in the

81 enterocyte lineage result in either asymmetric fate (one ISC and an EB), or

82 symmetric self-renewal (two ISCs) or differentiation (two EBs), which globally

83 result in balanced, homeostatic proportions (de Navascués et al., 2012) (Fig.

84 1D). This mode of tissue maintenance, whereby the balance between stem

85 cell self-renewal and differentiation is achieved at the population level rather

86 than within every stem cell lineage, is termed neutral competition (Klein and

87 Simons, 2011) and is found in a growing number of self-renewing adult

88 tissues (Simons and Clevers, 2011). While no molecular mechanism has been

89 fully elucidated so far for any case of neutral competition, in the fly gut it has

90 been proposed to arise from lateral inhibition mediated by Notch/Delta (de

91 Navascués et al., 2012), a pathway known to define the fate of the ISC

92 offspring (Ohlstein and Spradling, 2006; Micchelli and Perrimon, 2006; Bardin

93 et al., 2010).

94 Here we explore the capacity of a standard model of lateral inhibition acting in

95 pairs of interacting cells to result in steady states with different signalling

96 states (either symmetric or asymmetric) coexisting in the tissue. We find that

97 this is indeed possible, provided signalling thresholds vary across cell pairs.

98 Next, we turn to the *Drosophila* midgut and find that the tissue displays high

99 variability of contact area between pairs of ISC/EB cells, which can be

100 associated to an effective heterogeneity in signalling thresholds between pairs

101 of cells. When contrasting this variability with the distribution of fate

102 combinations in pairs of ISC/EB cells, we find a correlation between contact

103 area of specific cell pairs and their fate profile. Moreover, our model can

104 reproduce the distribution of fate outcomes given the contact area distribution

105 determined experimentally.

106 Our results expand the repertoire of possible outputs of a system governed by

107 lateral inhibition, and connect this mode of signalling with a mode of stem-cell

108 based tissue maintenance (neutral competition) that is highly relevant in adult

109 tissue homeostasis and tumourigenesis (Simons and Clevers, 2011;

110 Vermeulen et al., 2013; Baker et al., 2014), and whose molecular regulation is

111 poorly understood.

112 **Materials and Methods**

113 *The model: lateral inhibition mediated by Notch-Delta interaction*

114 We consider that the rate of Notch activation in a cell is an increasing function

115 of Delta concentration on its neighbour (signalling), and that the rate of Delta

116 expression is a decreasing function of the level of activated Notch in the same

117 cell (inhibition). We represent these interactions by means of a standard

118 mathematical model of Notch/Delta signalling (Collier et al., 1996) between

119 pairs of cells, which is given by:

120
$$\frac{d\bar{N}_1}{dt} = \alpha f(\bar{D}_2) - \delta_N \bar{N}_1, \tag{1}$$

121
$$\frac{d\bar{D}_1}{dt} = \beta g(\bar{N}_1) - \delta_D \bar{D}_1, \tag{2}$$

122
$$\frac{d\bar{N}_2}{dt} = \alpha f(\bar{D}_1) - \delta_N \bar{N}_2, \tag{3}$$

123
$$\frac{d\bar{D}_2}{dt} = \beta g(\bar{N}_2) - \delta_D \bar{D}_2. \tag{4}$$

124 Here $\bar{N}_{1,2}$ represent the levels of Notch activity in cells 1 and 2, and $\bar{D}_{1,2}$ are

125 the concentrations of Delta in each cell. α and β are the maximal production

126 rates of Notch and Delta, respectively, whereas δ_N and δ_D are their

127 corresponding degradation rates. The production terms for Notch (f) and

128 Delta (g) are given by the Hill functions

129
$$f(\overline{D}) = \frac{\overline{D}^r}{K_N^r + \overline{D}^r}, \qquad g(\overline{N}) = \frac{1}{1 + (\overline{N}/K_D)^h},$$
(5)

130 where the first function represents the signalling effect of Delta on the

131 neighbouring cell, and the second corresponds to the inhibition of Delta

132 expression by activated Notch in the same cell. K_N is the threshold of Notch

133 activation by neighbouring Delta, K_D is the threshold of Delta inhibition by

134 Notch in the same cell, and the coefficients r and h represent the cooperative

135 character of the two aforementioned processes. Similarly to (Collier et al.,

136 1996) we rewrite Eqns 1- 4 in dimensionless form as:

137
$$\frac{dN_{1,2}}{dt} = \frac{D_{2,1}^r}{a^r + D_{2,1}^r} - N_{1,2}, \qquad \frac{dD_{1,2}}{dt} = v\left(\frac{1}{1 + \left(\frac{N_{1,2}}{b}\right)^h} - D_{1,2}\right)$$
(6)

138 The parameter v is the ratio between the degradation rates of Delta and

139 Notch, δ_D/δ_N. a and b are the dimensionless thresholds for Notch activation by

140 Delta in the neighbouring cell, and Delta inhibition by Notch in the same cell,

141 respectively,

142
$$a \equiv \frac{K_N \delta_D}{\beta} \equiv \frac{c}{A}, \qquad b \equiv \frac{K_D \delta_N}{\alpha}.$$
(7)

143 a and b are referred to as the activation and inhibition thresholds, and their

144 values set the location of the half-maximal points of the Hill functions in Eqn 6.

145 Importantly, the signalling threshold a is considered to depend explicitly on the

146 contact area A between the two interacting cells, since a larger contact area

147 will effectively reduce the threshold of Notch activation, by increasing the

148 number of receptors available to bind ligands from the sending cell. The

149 constant c is treated as a parameter of the model.

150 We studied the behaviour of the system on a region of the a-b parameter

151 space that spans a biologically plausible range, according to data from the

152 literature for K_N (Sprinzak et al., 2010; Pei and Baker, 2008), K_D (Friedmann

153 and Kovall, 2010), α, β (Agrawal et al., 2009), δ_N (Hsu et al., 2006; Agrawal et

154   al., 2009), and δ_D (Hsu et al., 2006). For fixed Hill coefficients r and h, the

155   parameters a and b determine the steady state of the system.

156   *Steady states and cell fate identification*

157   The system of equations (6) has a homogeneous steady state in which Notch

158   and Delta have the same values in the two cells:

159   $$N^* = f(D^*), \qquad D^* = g(N^*)$$

160   This state corresponds to a situation in which both cells in the pair have the

161   same fate. The stability boundary of this homogeneous steady state can be

162   calculated using standard methods (Collier et al., 1996), and is represented by

163   a dotted line in Fig. 2A. Above this line the homogeneous state is stable.

164   Below it, a heterogeneous stable steady state appears in which the values of

165   Notch and Delta are different between the two cells:

166   $$N_1^* = f(D_2^*), \qquad D_1^* = g(N_1^*),$$

167   $$N_2^* = f(D_1^*), \qquad D_2^* = g(N_2^*).$$

168   In parallel with this classification of steady states, a cell is considered to be

169   Notch positive when the level of Notch surpasses a certain threshold N_{thr}

170   (considered here to be 0.1), and Notch negative in the opposite case. In the

171   case of the *Drosophila* midgut, a Notch positive cell would correspond to an

172   EB, and a Notch negative cell to an ISC. In that way, a homogeneous steady

173   state can represent either an ISC/ISC pair (symmetric Notch negative, blue

174   region in Fig. 2A) or an EB/EB pair (symmetric Notch positive, green region in

175   Fig. 2A). Most heterogeneous steady states, in turn, correspond to an ISC/EB

176   pair (orange region in Fig. 2A), although heterogeneous states in which both

177   values of Notch lie below (or above) the threshold N_{thr} still represent

178   symmetric ISC/ISC (or EB/EB) pairs. This is reflected in Fig. 2A through the

179   difference between the stability boundary (dotted grey line) and the

180   boundaries between the fate-pair domains shown in colour code.

181   *Dynamical behaviour*

182   We investigate the temporal evolution of the model by solving numerically the

183   Equations (6). For this purpose, we use a finite difference approximation (two-

184   stage Runge-Kutta; LeVeque, 2007). In our calculations, we are considering

185   $r = h = 2$ and $\delta_N = \delta_D$, as in previous works (Collier et al., 1996; Sprinzak et

186   al., 2010). Cells are considered initially negative for Notch activation (Ohlstein

187   and Spradling, 2007; Guo and Ohlstein, 2015).

188   *Drosophila culture and strains*

189   Adult flies were raised in standard cornmeal medium, collected daily and

190   maintained in fresh vials with added yeast (food replaced every 24-48h).

191   Untreated flies were dissected at 4-6 days of age. Mifepristone (RU486)

192   treated flies were treated as described above and transferred to RU486-

193   containing medium at 3-8 days of age for three more days before dissection.

194   EBs were identified by co-expression of one of two enhancer trap reporters of

195   the undifferentiated cell marker *escargot* (FlyBase: *P{PTT-GB}esg*[YB0232];

196   Quiñones-Coello et al., 2007; or *P{lacW}esg*[k00606]; Spradling et al., 1999) and

197   one of two *GBE-Su(H)* synthetic reporters of Notch transcriptional activity

198   (Bray and Furriols, 2001; de Navascués et al., 2012) while ISCs were

199   identified by expression of the *esg* reporter alone (Micchelli and Perrimon,

200   2006; Ohlstein and Spradling, 2006).

201   Delta levels were measured with the *Delta*[MI04868-GFSTF.1] transgenic insertion

202   (FlyBase *Mi{PT-GFSTF.1}Dl*[MI04868-GFSTF.1]), which tags all three annotated

203   Delta isoforms with GFP at the endogenous locus (Nagarkar-Jaiswal et al.,

204   2015).

205   Genetic perturbation of Notch activity was performed (1) by knockdown with

206   *da-GS* (FlyBase: *P{da-GSGAL4.T}*; Tricoire et al., 2009) and *UAS-Notch*[RNAi]

207   (FlyBase: *P{w[+mC]=UAS-N.dsRNA.P}14E*; Presente et al., 2002), activated

208   with mifepristone (RU486, Sigma), with mock treatment as control, or (2) by

209   using the molecular null allele *N*[55e11] (Kidd et al., 1983) or the Delta-

210   dependent, hypermorphic *l(1)N*[B] (FlyBase: *N*[l1N-B]; Lyman and Young, 1993;

211   Brennan et al., 1997), with *Oregon R* as wild-type control.

Immunohistofluorescence and imaging

213 Immunofluorescence was performed essentially as described in (Bardin et al.,

214 2010) but with a heat fixation step (Miller et al., 1989). This fixation method

215 was essential for the robust immunodetection of Armadillo (Fang et al., 2016).

216 Primary antibodies were: chicken anti-β-Galactosidase (Abcam ab9361,

217 1:200), rabbit anti-GFP (Abcam ab6556, 1:200), sheep anti-Notch (Muñoz-

218 Descalzo et al., 2011; 1:1000), anti-Arm (mAb N2-7A1, 1:50) and anti-Dl (mAb

219 C594.9B, 1:50). The N2-7A1 and C594.9B antibodies were obtained from the

220 Developmental Studies Hybridoma Bank (NICHD and The University of Iowa).

221 Secondary antibodies conjugated with Alexa fluorophores were from

222 Invitrogen (1:500). Of note, immunodetection of *GBE-Su(H)-lacZ* expression

223 in heat-fixed material was less sensitive than that of *GBE-Su(H)-GFP:nls*; this

224 might have led to an underestimation of EBs numbers, which in any case will

225 have played against our hypotheses.

226 Confocal stacks were obtained in a Zeiss LSM 710 with an EC Plan-Neofluar

227 40X oil immersion objective (numerical aperture 1.3). For the quantification of

228 membrane features, voxel sizes were 0.22x0.22x0.6, 0.21x0.21x1, or

229 0.18x0.18x0.6 (contact area), 0.16x0.16x0.7 μm (distribution of Notch and

230 Armadillo), or 0.14x0.14x1 μm (distribution of Delta), with airy units adjusted

231 so that there was negligible oversampling in Z, or not at all.

232 *Image analysis*

233 To measure contact area, stacks were analysed with a combination of ImageJ

234 macros and python scripts to (1) manually identify all esg-GFP$^+$ cells in a z-

235 projection of the stack, (2) automatically threshold *GBE-Su(H)-lacZ* reporter

236 expression in 3D to determine its expression status (positive or negative) in

237 every esg$^+$ cell, followed by a step of manual correction, (3) manually identify

238 the nests of esg$^+$ cells so that (4) a series of 3D stacks, containing only one

239 pair each, is automatically cropped, and (5) the contact membrane of each

240 esg$^+$ cell pair is semi-automatically determined using FIJI for each optical

241 plane, by binarising the immunofluorescence of Armadillo/*β*-catenin (Arm).

242 Arm labels the membrane throughout the apical-basal axis (see Results),

243 which allows measuring the amount of contacting membrane in each cell pair

244 as the number of Arm$^+$ voxels shared between the two cells (expressed in

245 μm^2).

246 To measure cell size, the cellular perimeter in 3D was used to measure the

247 volume enclosed. Alternatively, we projected the maximum intensity of Arm in

248 the Z dimension and calculated the area enclosed in the projected perimeter

249 of the cell as the 'projected area'. This measurement correlated well with the

250 cell volume (Fig. S6A).

251 To evaluate the co-localisation between Delta:GFP and anti-Delta, Delta$^+$ cells

252 appriopriately immunostained were manually identified and individually

253 outlined in 2D in several fields of view (comprising a few hundred enteric cells

254 each). For each outline, the enclosing 3D stack was automatically extracted,

255 and the Pearson correlation and the Manders co-localisation (Manders et al.,

256 1993) coefficients were calculated between different pairs of channels.

257 For measuring Notch, Delta and Arm distribution at the membrane, the

258 membrane contours (3-4 pixels wide) of cells in pairs were manually

259 determined in each plane. At the spatial resolution of our micrographs, it is not

260 possible to distinguish, for a pixel at the boundary, to which cell of the pair it

261 belongs, so we took the approximation of splitting the thickness of the contact

262 between the two cells. Intensity data from those positions were used as

263 described in what follows.

264 *Intensity normalisation.* For each plane in the confocal stack, an empty 50x50

265 pixel square nearby each of the cell pairs in that stack was manually selected.

266 The signal therein (for all the planes in the stack where membrane was

267 detectable) was averaged for all the squares of the same stack, and this value

268 was taken as background. Notch, Delta and Arm intensity values for each

269 stack were normalised by dividing by the background value.

270 *Distribution along cell perimeter.* In each confocal plane, each membrane

271 pixel position was assigned an angular value respect to the centroid by

272   calculating its tangent arc (±π depending on the quadrant). Thirty overlapping

273   sliding windows (of 2π/15 rad with half window overlap) were delimited in each

274   plane, and their pixel intensities were normalised and averaged.

275   *Distribution along the apical-basal axis.* Each cell was sliced in 10 overlapping

276   angular windows (2π/5 rad with half overlap). For each window, a normalised,

277   average intensity measurement was taken per confocal plane (i.e. along the

278   apical-basal axis). Apical-basal positions were normalised from 0 to 1.

279   Intensity data points along the apical-basal axis were obtained by interpolation

280   from average normalized intensity values.

281   **Results**

282   <u>*Lateral inhibition can result in stable, opposing symmetric signalling states*</u>

283   We study the steady-state behaviour of a standard model of lateral inhibition

284   for the case of two cells (see Methods). For fixed r and h, the steady states of

285   this system depend on two parameters, a and b (the dimensionless activation

286   and inhibition thresholds, respectively; see Methods), which we allow to vary

287   across the population of cell pairs. We then calculate the equilibrium state of

288   the system in this two-dimensional parameter space, according to the

289   resulting signalling profile: asymmetric (one cell positive for Notch activation

290   and the other one negative, see Methods), symmetric positive, or symmetric

291   negative for Notch activation (Fig. 1C). Thus, for a population of cell pairs with

292   variable activation or inhibition thresholds (a and b), the three possible

293   signalling state profiles occur (Fig. 2A, see Fig. 2B-E for a comparison of the

294   dynamic evolution of examples of the three profiles, with Fig. 2B

295   corresponding to the parameter values from Collier et al., 1996). The three

296   signalling state profiles can be found within a relatively short range of

297   parameter values (Fig. 2A). Importantly, this scenario does not change

298   qualitatively when considering a wide range of threshold values for Notch

299   activity classification, as defined in the Methods section ($0.001 \leq N_{thr} \leq 0.8$;

300   Fig. S1B-E), or higher cooperativity values in Notch signalling or Delta

301   inhibition ($r, h = (2, 5)\ or\ (5, 2)$) (Fig. S1F-G). However, we found that

302 cooperativity was necessary: for $r = 1$, $h = 1$, the heterogeneous

303 (asymmetric) steady states are lost (Fig. S1H). This requirement of

304 cooperativity is in agreement with other theoretical works on lateral inhibition

305 (Sprinzak et al., 2011) as well as with *in vitro* estimates for r of 1.7 (Sprinzak

306 et al., 2010).

307 In a biological system, the existence of three possible signalling state profiles

308 would be equivalent to having three different cell fate combinations across a

309 population of initially uncommitted cell pairs interacting through Notch/Delta,

310 with the specific fate combination of a given cell pair depending on the

311 sensitivity to Delta activation and Notch inhibition of the pair. To investigate

312 the potential of this lateral inhibition model, incorporating variable activation

313 and inhibition thresholds, to describe a real biological system, we turned to the

314 *Drosophila* midgut.

315 *Cell pair type frequencies correlate with Notch activity*

316 As mentioned in the Methods section, in the *Drosophila* midgut Notch

317 negative cells correspond to ISCs, and Notch positive cells to EBs. The Notch

318 activity reporter *GBE-Su(H)* is hardly expressed above background levels in

319 ISCs (Ohlstein and Spradling, 2007; and our own observations), and hence

320 our choice of a low threshold value, $N_{thr} = 0.1$. Symmetric positive pairs in the

321 model will equate to an event of symmetric differentiation (EB/EB), symmetric

322 negative pairs to symmetric self-renewal (ISC/ISC), and asymmetric pairs to

323 asymmetric ISC fate (ISC/EB) (Fig. 2A). If this was the case, we would expect

324 the relative frequencies of these pairs to correlate with overall *Notch* activity

325 levels, as has been shown with the balance of the whole population of ISC

326 and EB levels (Biteau et al., 2008; de Navascués et al., 2012). Indeed,

327 heterozygous conditions for the null allele N^{55e11} lead to more ISC-ISC pairs

328 and less EB-EB pairs relative to the wild-type, whereas heterozygosis for the

329 hyperactive, Dl-dependent *l(1)N^B* mutation favours EB-EB pairs at the

330 expense of ISC-ISC pairs, whose presence is negligible (Fig. 1E). To ensure

331 that these differences are due to variations in Notch activity, rather than to the

332 genetic background of the different mutant chromosomes, we did a serial

knock-down of *Notch* in ISCs and EBs. To that end, we used the GeneSwitch

system (Osterwalder et al., 2001) with the driver *da-GS*, which is largely

specific of ISCs and EBs in the intestine (Fig. S2A and Nicolas Buchon,

personal communication), and increasing concentrations of the inducer

RU486. In these experiments, the flies share the same genetic background,

and only differ in the amount of RU486 present in the food. Indeed, we find

that mild knock-down of *Notch* (to a level that does not yet lead to ISC-like

tumour growth; Fig. S2B-F), increases the number of ISC-ISC pairs at the cost

of ISC-EB and EB-EB pairs, in a dose-dependent manner (Fig. 1F). Note that

the baseline fractions of the control for the induction experiment ('mock' bars

in Fig. 1F) are different from the control for the mutants ('$N^{+/+}$' bars in Fig. 1E),

even if at the overall level the total numbers of ISCs and EBs are balanced

(Fig. 1G, H; de Navascués et al., 2012), highlighting the importance of

controlling for genetic background in these experiments. From these data we

conclude that the frequency of undifferentiated pair types are a good readout

of the strength of Notch signalling.

Cell contact area as modulator of activation threshold

To relate the model to real tissue, we need first to consider how the

dimensionless parameters a and b are related to biological features displaying

variability across undifferentiated (esg$^+$) cell pairs. We assume that

biochemical processes intrinsic to the cell, such as protein degradation rates

(δ_D and δ_N), the maximal biosynthesis rates (α and β), and the threshold of

Delta inhibition by Notch in the same cell (K_D), will not be highly variable

among cells with a common developmental identity. On the other hand, the

threshold of Notch activation by neighbouring Delta (K_N) depends directly on

the interaction between the two cells, which could be variable for different

pairs of cells. For instance, due to spatial heterogeneity of cell packing, the

contact area between cell pairs could be substantially different from pair to

pair. Indeed, tissue images reveal that undifferentiated cells in nests show

irregular shapes and variable contact area (Fig. 3A). In the Notch/Delta

system the amounts of Notch and Delta are usually limiting, and this seems to

364 hold true for the adult *Drosophila* gut, where haploinsufficiency has been

365 described (Biteau et al., 2008; de Navascués et al., 2012; see also Fig. 1E-H).

366 Therefore, it is expected that variations of ~2-fold or more in contact area

367 would lead to significant changes in the levels of Notch activation. This is

368 captured in the model by expressing the dimensionless activation threshold a

369 in terms of the contact area, following Eqn 7 above. Specifically, we assume

370 that a is inversely related with the contact area (the larger the contact area,

371 the easier it is for Delta to activate Notch, and thus the smaller the activation

372 threshold). As shown in Fig. 2A (see also Fig. S3), variation in a best allows

373 for heterogeneity in stable steady state levels of Notch activity and therefore in

374 fate choice. From this we hypothesize that variation of contact area (or any

375 other biological feature correlating with the threshold of Notch activation) is

376 likely to allow the diversity in fate outcome predicted by the model.

377 The above-mentioned assumption by which the activation threshold depends

378 inversely on the contact area requires Notch and Delta proteins to be

379 homogeneously distributed across the cell surface (such that their probability

380 of binding increases with the area of contact). To evaluate this, we used

381 confocal microscopy to examine the localisation of both Notch and Delta

382 proteins respect to the membrane marker Armadillo/β-catenin (Arm), in both

383 single and paired ISCs and EBs in the midgut epithelium (Fig. 3B-C). In

384 *Drosophila* epithelia, Arm/β-cat participates in the formation of adherens

385 junctions, which localise mostly in the apical domain, with lower levels at the

386 lateral membrane (Tepass and Hartenstein, 1994). Therefore, we used Arm

387 staining to define membrane boundaries in 3D, and measured the intensity of

388 Arm, Notch, and Delta:GFP proteins at the cell membrane. The latter is an

389 endogenously tagged protein which correctly represents the localisation of the

390 wild-type Delta both visually and by co-localisation analysis (Fig. S4; see also

391 Nagarkar-Jaiswal et al., 2015).

392 We could not find any strong pattern in the variations of Notch or Delta

393 immunodetection intensity within confocal planes, and it would only seem that

394 both are slightly enriched at the boundary between two undifferentiated cells

395 (Fig. 3E-F). This indicates that Notch and Delta concentrations are largely

396 independent of the position at the membrane along the cell perimeter, and in

397 particular along the contact between esg$^+$ cells. Moreover, the localisation of

398 both Notch and Delta along the apical-basal axis of the cells is also largely

399 homogeneous (Fig S5E,F). This is manifest in the small variation in the

400 average amounts of Notch and Delta between different optical planes (Fig.

401 S5B-C, left panels), and in the narrow distribution of mean values per plane,

402 with low values of coefficients of variation per plane, of Notch intensity values

403 (Fig. S5B-C, right panels). Therefore, the contact area between cells is a good

404 approximation to the total amount of Notch and Delta proteins available for

405 signalling.

406 We note that Arm largely parallels Notch and Delta localisation at the

407 membrane (Figs. 3D and S5D) but shows a stronger enrichment at the

408 boundary (Fig. 3D), in agreement with previous reports (Maeda et al., 2008).

409 Incidentally, these results also reveal that neither Arm nor Notch nor Delta are

410 restricted to the apical domain in the midgut epithelium, and instead can be

411 found in similar amounts along the apical-basal axis of the membrane in ISCs

412 and EBs (Fig. S5D-F). This situation contrasts with Arm and Notch distribution

413 in other Drosophila epithelia (Tepass and Hartenstein, 1994; Tepass et al.,

414 2001; Sanders et al., 2009).

415 Taken together, our results suggest that both the Notch receptor and its ligand

416 Delta are randomly and homogeneously distributed in the cell membrane,

417 which suggests that measurements of membrane contact area may be

418 relevant to the dynamics of Delta-Notch signalling as a proxy for the activation

419 threshold a in our model.

420 *Correlation of contact area values and cell fate profiles*

421 We have shown that contact area can be used as a measure of the amount of

422 Notch and Delta available for interaction. Therefore, our model predicts that

423 contact area should correlate with the patterns of symmetric and asymmetric

424 fates. Indeed, we observe increasing average contact area in ISC-ISC

425 (7.67μm^2), ISC-EB (13.28μm^2) and EB-EB (14.79μm^2) cells (Fig. 4A). The

15

426 contact area in ISC-ISC pairs was significantly lower than in the other two cell-

427 pair types (with *p*-values of 0.002 and 0.005 when compared with ISC-EB and

428 EB-EB pairs, respectively), while the latter could not be statistically

429 distinguished from each other (*p* = 0.5). We must also remark that EB cells

430 increase in size after they progress from their original ISC state (Fig. 4B and

431 S6B), which complicates our interpretation of the correlation between fate and

432 contact area, especially in EB-EB pairs. This fact, together with the statistical

433 similarity between ISC-EB and EB-EB pairs mentioned above, led us to focus

434 on the distinction between ISC-ISC and ISC-EB, filtering the results coming

435 from the latter cell-pair type based on the size of the EB cells (see below).

436 We measured the contact areas in 480 pairs of esg$^+$ cells with both symmetric

437 (ISC-ISC, n=74) and asymmetric (ISC-EB, n=406) fates. The data show that

438 contact area in these pairs is highly variable, ranging from just around 1μm^2 to

439 over 40μm^2 (Fig. 4C). This degree of variability (of more than one order of

440 magnitude) indicates that contact area has the potential to be a regulatory

441 mechanism of the system (through its influence on the dimensionless

442 activation threshold a).

443 Next, we classified measurements of contact area according to the fate profile

444 of their corresponding cell pair and compared their values (Fig. 4D). We found

445 that the cumulative distributions of contact areas in ISC-ISC and ISC-EB pairs

446 are clearly separated. On average, the contact area between two ISCs (11.59

447 ± 0.73 μm^2; mean ± standard error of the mean) is clearly smaller than that

448 between an ISC and an EB (17.68 ± 0.42 μm^2) ($p = 8\times10^{-7}$). To verify that this

449 correlation is not simply a consequence of EBs being larger, we compared the

450 distributions of contact areas between ISC-ISC pairs and different subsets of

451 ISC-EB pairs which included only the pairs where the EB member was smaller

452 than a given size limit (1x, 0.75x and 0.5x the maximum ISC size,

453 respectively). The effect of the thresholding on the distribution of cell sizes

454 (measured in terms of the projected areas) is shown in Fig. 4E. Note that as

455 the threshold decreases the average size of the filtered EBs is progressively

456 smaller, until it can no longer be statistically discriminated from the distribution

457 of ISC sizes (for the subset with size limit equal to half the maximum ISC size,

458 $p = 0.07$). However, the corresponding contact area distributions of these

459 subsets of ISC-EB pairs are all strikingly similar, with values systematically

460 larger than those of ISC-ISC pairs at a high level of significance (maximum p-

461 value = 2×10^{-4}) (Fig. 4F). This is in good agreement with the fact that the cell

462 size of the pair members and their contact area are not correlated (Fig. S6C-

463 D).

464 We also wanted to check that the differences in cell-pair types discussed

465 above are not associated with differences in adhesion properties between

466 ISCs and EBs, as could be suggested by the fact that Arm levels are enriched

467 at the contact area between these cell pairs (Fig. 3D). For this, we measured

468 the values of Arm at the boundary of ISC-ISC pairs and ISC-EB pairs. Since

469 we cannot distinguish which cell of the pair originates the Arm signal at the

470 boundary (see Materials and Methods), we measured the signal assigned to

471 ISCs in either ISC-ISC pairs or ISC-EB pairs, as an approximation to the

472 strength of adhesion at the boundary of these cell pairs. We found a similar,

473 moderate increment in Arm levels at the cell pair boundary in both ISC-ISC

474 and ISC-EB pairs (Fig. S6E-F), indicating that adhesion properties are not

475 fundamentally different between cell pair types (at least as far as adherens

476 junctions are concerned). This fits well with the observation that the

477 transcriptional profiles of ISCs and EBs are not particularly enriched in genes

478 involved in cell adhesion (Dutta et al., 2015).

479 Taken together, these results indicate that a smaller contact area correlates

480 with the ISC-ISC pair profile, and this is likely linked to a higher activation

481 threshold of Notch in ISC-ISC pairs, rather than to changes in cell shape, size

482 or adhesion properties in the ISC-EB pairs posterior to EB fate acquisition.

483 *Updating the model with area variation reproduces fate profile distributions*

484 This finding gives us biological justification to consider the activation threshold

485 a to be variable in the model (inversely proportional to the contact area), and

486 test the capacity of the model to produce the observed proportions of fate

487 pairs in our various experimental conditions (Fig 1E, F). To do this, we first

488 generated a large sample of contact area values A, from a Smooth Kernel

489 Distribution based on the experimental data (Fig. 4C). To input values from A

490 into the model, we simply used Eqn. 7 ($a \equiv c/A$). We then analysed the stable

491 steady states of the model, obtaining the proportions of the three possible fate

492 pairs resulting from A, for different values of b and c.

493 In order to compare the fate distribution obtained from the model and the

494 experimental datasets we use the Kullback-Leibler relative entropy (H), which

495 is a dissimilarity measure between two probability distributions (giving the

496 value 0 if the distributions are equal; Kullback and Leibler, 1951). We found an

497 excellent agreement between the proportions of EB-EB, EB-ISC and ISC-ISC

498 pairs observed experimentally, and the distributions from the model for an

499 extended range of values of b and c, as indicated by the low values of H

500 between theoretical and experimental distributions (see Fig. S6G-H). Ranges

501 of values for parameters a and b with good fit for each experimental condition

502 are mapped to the model phase diagram in Fig. 4G (upper panel for *Notch*

503 mutant and wild-type alleles; lower panel for RU486-induced *Notch* knock-

504 down and the mock treatment), with corresponding pair frequencies (data and

505 model) and parameter values (c, average b) given in Table 1 (with H values

506 ranging from 1.8×10^{-4} to 1.6×10^{-2}). Focusing on the control datasets (*Notch*

507 wild-type and *Notch* mock knock-down, Fig. 4G) one finds that ISC-ISC pairs

508 occur at the lowest values of contact area (largest values of a), in good

509 agreement with our experimental observations (Fig. 4A, D, F). In this region of

510 parameter space, EB-EB and ISC-EB pairs are found at higher values of

511 contact area (lower a), although we cannot distinguish statistically between

512 the experimentally measured contact areas of these two cell-pair types (Fig.

513 4A). Importantly, we find that the regions of the parameter space where the

514 model fits each of the mutant and knockdown experimental distributions

515 correspond to parameter changes in line with the nature of the genetic

516 perturbations. First, for all loss-of-function conditions of *Notch* (*Notch*

517 knockdown and $N^{55e11/+}$ heterozygotes), the model can account for the

518   observed pair frequencies with small shifts in the b parameter and more

519   substantial changes in the a parameter (note the very different scale ranges

520   for a and b in Fig. 4G). The shifts towards higher a values can be explained

521   as an increase in the K_N parameter (i.e. lower activation of Notch for a given

522   Delta stimulus; see Eqns. 5 and 7), which fits the nature of a loss of function

523   condition. In the case of *Notch* gain of function, represented by the $N^{l1N-B/+}$

524   hypermorphs, the model can reproduce the resulting pair frequencies by

525   substantially reducing both a (therefore decreasing K_N, i.e. more Notch

526   activation for the same Delta stimulus) and b (which can be accounted for as

527   an increase of α, the maximal rate of Notch activation; see Eqn. 7); again,

528   both notions sit well with the nature of the *l(1)N^B* allele (a Delta-dependent,

529   hypermorphic allele).

530   Our experimental observations thus agree with the model predictions,

531   including both gain and loss of function perturbations of Notch signalling.

532   Hence, our results confirm that the contact area between pairs of cells can

533   influence the fate outcome of Notch/Delta signalling in the *Drosophila* midgut

534   (Fig. 4H), with small contact area clearly favouring symmetric self-renewal.

535   **Discussion**

536   We have considered a standard model of Notch/Delta-mediated lateral

537   inhibition (Collier et al., 1996) and investigated the effect of the trans-

538   activation of Notch by Delta and the inhibition threshold of Delta by Notch

539   signalling (here considered phenomenologically as the dimensionless

540   thresholds a and b, respectively) on the dynamics of lateral inhibition for a

541   system of two cells. We find that, provided there is a degree of variability in

542   contact areas between cell pairs, three different signalling states (and

543   therefore fate combinations) can occur under the same conditions. This is a

544   considerable expansion of the model, whose use has so far been mostly

545   centred on solutions that provide fine-grained (checkerboard) patterns. The

546   model reproduces the signalling outcomes observed in the *Drosophila*

547   intestine, which translate into differentiation vs. self-renewal fates. Thus, our

548   results provide a mechanism whereby ISCs may undergo neutral competition,

19

549 which is a widespread pattern of adult tissue maintenance in metazoans from

550 *Drosophila* to humans.

551 The work by Collier et al. (1996) established a minimal model of lateral

552 inhibition as a system leading to checkerboard patterns of stable, all-or-none

553 signalling states. Their formalisation, and choice of parameters, has become a

554 reference in the field (Sprinzak et al., 2011; Formosa-Jordan et al., 2012;

555 Petrovic et al., 2014). However, to allow accommodating phenomenology that

556 departs from the classical fine-grained, all-or-none patterns, expansions of

557 this model have required the introduction of additional genetic components

558 (e.g. an extra ligand; Boareto et al., 2015) or noise components (de Back et

559 al., 2013). By contrast, here we have left intact the general dynamics of the

560 minimal model and simply introduced a degree of variability in the sensitivity

561 of each cell pair to signal transduction.

562 Our work considers the contact area between cells engaged in signalling as

563 the source of variation in signalling threshold. Contact area can be an

564 effective tuning parameter of a biological system (Khait et al., 2015), since it

565 can integrate mechanical constraints into signalling, as it has been shown for

566 cell density and proliferative control by the Hippo pathway (Schlegelmilch et

567 al., 2011; Kim et al., 2011; Silvis et al., 2011). In a system such as the

568 posterior midgut, where some differentiated cells are much larger than their

569 progenitors (see Fig. 1A), differentiated and mature cell loss certainly would

570 have a local impact in the packing geometry of cells interacting via

571 Notch/Delta, and connect naturally with the fate outcome of stem cell

572 divisions. This could be particularly useful in conditions of regeneration.

573 Importantly, our theoretical framework could in principle accommodate any

574 source of variation; for instance, variation arising from the unequal (either

575 random or regulated) inheritance of signalling components could result in

576 variation in the capability of signal transduction in the population. It is

577 interesting to consider that while shortly after division most of the ISC

578 daughter cells display similar levels of Notch and Delta proteins (Ohlstein and

579 Spradling, 2006), endosomes bearing the signalling molecule Sara display an

580 inhomogeneous inheritance pattern (Montagne and González-Gaitán, 2014).

581 It has recently been found that ISC divisions producing enteroendocrine cell

582 precursors do seem to segregate Delta asymmetrically towards the precursor

583 cell (Guo and Ohlstein, 2015), which suggests that ISCs switch between

584 different types of cell division.

585 Understanding how Notch/Delta signalling results in stochastic cell fate

586 patterns is of particular relevance in adult homeostatic tissues, as Notch

587 signalling controls fate in many types of tissue stem cells (Koch et al., 2013).

588 Moreover, many adult stem cells balance their fate via neutral competition

589 (Krieger and Simons, 2015). Our model proposes a mechanism whereby

590 Notch/Delta signalling could result in neutral competition of stem cells by

591 lateral inhibition between sibling cells. This provides an alternative explanation

592 to the neutral competition of *Drosophila* adult ISCs, which has been proposed

593 to arise from Notch/Delta-mediated lateral inhibition involving the offspring of

594 non-related ISCs, coinciding in space (de Navascués et al., 2012) and

595 resolving 20% of the time in symmetric fate. Although the two proposals are

596 compatible with each other, the latter faces the difficulty that ISC/EB nests

597 rarely contain more than two cells (de Navascués et al., 2012). Moreover, we

598 and others have found isolated pairs of ISCs or EBs frequently in the tissue

599 (de Navascués et al., 2012; Goulas et al., 2012). Our model provides a

600 potential explanation of how the offspring of a single ISC (pairs of Notch/Delta

601 signalling cells) may reach a symmetric steady state, leading to symmetric

602 self-renewal or differentiation.

603 It would be interesting to see how our model translates to a larger group of

604 interacting cells, in particular in light of recent findings in the oesophageal

605 epithelium. There, tissue is maintained by the neutral competition of basal

606 progenitor cells (Doupé et al., 2012), and this competition is heavily influenced

607 by Notch signalling, to the point that alterations in the pathway can lead to the

608 fixation of mutant clones and poise the tissue for tumour initiation (Alcolea et

609 al., 2014).

610 **Acknowledgements**

21

618 **Competing Interests**

619 No competing interests declared.

620 **Figure Legends**

621 **Figure 1**. Tissue maintenance in the *Drosophila* adult midgut and effect of

622 mild genetic perturbations of Notch signalling. Scale bars: 20μm. **A**. Confocal

623 micrograph showing the cell types present in the midgut epithelium. ISCs are

624 esg-GFP$^+$ (blue) and EBs are esg-GFP$^+$ and GBE-Su(H)-lacZ$^+$ (green). The

625 two differentiated cells, enteroendocrine cells and enterocytes, are

626 recognisable by Prospero (Pros) expression and having large, polyploid nuclei

627 (Hoechst, grey), respectively. **B**. ISCs self-renew and produce EBs (which will

628 terminally differentiate without further division). **C**. Confocal micrographs

629 showing examples of cell pair type profiles: asymmetric (i), symmetric Notch

630 negative (two ISCs, ii) and symmetric Notch positive (two EBs, iii). **D**. ISCs

631 balance self-renewal and differentiation by dividing either asymmetrically (one

632 ISC and an EB), or symmetrically into two ISCs or two EBs. **E**. Observed

633 frequencies of the pair types depicted in C, D for wild type (n=235),

634 hypermorphic (*l(1)N^B/+*, n=209) and hypomorphic (*N$^{55e11/+}$*, n=213) conditions

635 for *Notch*. **F**. Observed frequencies of the pair types depicted in C, D for *da-*

636 *GS, UAS-N^{RNAi}* flies after three days of feeding on 0 ("mock", n=234), 20

637 (n=192) and 50μg (n=99) per vial of RU486. **G**. Total numbers of ISCs and

638 EBs in the pairs in the conditions described in E. Overall numbers of

639 ISCs/EBs in these genotypes are 765/737 (wild type), 790/752 (*N$^{55e11/+}$*) and

640 804/1148 (*l(1)N^B*) (de Navascués et al., 2012). **H**. Overall numbers of ISC/EB

641 in the conditions described in F. In E-H, triangles with colour gradient indicate

642 the relative levels of Notch signalling: wild-type (white), excessive (red) or

643 defective (blue).

644 **Figure 2**. Parameter space and dynamic behaviour of the model. **A**. Stable

645 solutions of the system classified according to their resulting signalling state.

646 Green stands for symmetric positive fates (EB-EB pairs), blue represents

647 symmetric negative fates (ISC-ISC pairs), and orange denotes asymmetric

648 fates (ISC-EB pairs). The threshold in Notch level for EB identification is taken

649 to be equal to 0.1 (see the text for more details). Dotted line, boundary of

650 stability for steady states with identical cells; these 'homogeneous' solutions

651 are stable above the line. **B-E**. Time evolution (in arbitrary units) of Notch and

652 Delta activity in pairs of cells interacting with parameters from the points

653 indicated as 1 to 4 in (A). Parameter values in point 1 correspond to those

654 used in Collier et al. (1996) (B), while parameter values in points 2-4 (C-E)

655 correspond to examples of other asymmetric pairs, and symmetric positive

656 and symmetric negative pairs.

657 **Figure 3**. Variability in contact area, and distribution of Notch and Delta at the

658 membrane. **A**. Confocal stacks projected in Z, showing variability in contact

659 length (as proxy for area). Scale bar: 20μm. **B**. (i, ii) Side views of the

660 intestinal epithelium, showing the apical-basal distribution of Notch and Arm.

661 Lumen is at the top and basal at the bottom. (iii-v) Top view of the intestinal

662 epithelium (iii) with ZY and XZ side views (iv, v) corresponding to the marked

663 lines in (iii). Lumen is at the top and right of the XZ and ZY views,

664 respectively. **C**. Top view of the intestinal epithelium, with ZY and XZ side

665 views corresponding to the marked lines in the top view panel. The top view

666 panel is a z-projection illustrating the membrane localisation of Delta, with side

667 views showing its apical-basal distribution. Lumen is at the top and right of the

668 XZ and ZY views, respectively. Scale bars in B, C are 10μm. **D-F**. Arm (D),

669 Delta (E) and Notch (F) levels along the perimeter of the cell planes (colour

670 lines) and mean (white). For each cell plane, position 0 corresponds to the

671 centre of the contacting membranes (defined as the position that intersects

the line connecting the cell centroids in that plane). Data in D and F are from 20 paired cells; data in E are from 43 cells.

Figure 4. The model can reproduce the observed cell fate profiles. Statistical comparisons between data distributions in A-B, D-F were performed with the Kolmogorov-Smirnov test. **A**. Swarm/box plots showing contact area values segregated by fate profiles (11 ISC-ISC, 218 ISC-EB and 42 EB-EB pairs). See main text. **B**. Swarm/box plots showing cell size values (measured as projected areas) of ISCs and EBs. Projected areas correlate well with cell volumes (Fig. S6A), which also shows a similar difference between ISCs and EBs (Fig. S6B). **C**. Frequency of contact area values for nests of two undifferentiated cells, irrespective of pair type. The red line marks the Smooth Kernel Distribution (SKD) used to generate areas for the simulation. **D**. Cumulative frequency of the contact area data for ISC-ISC and ISC-EB pairs. **E**. Cumulative frequency of cell size (projected area) of ISCs and EBs. Blue and light green lines correspond to the data depicted in B. Increasingly darker green lines correspond to the cell size distributions of EBs which are smaller than 1.0, 0.75 and 0.5 times the maximal ISC size, respectively. **F**. Cumulative frequency of contact area of ISC-ISC (blue line) and ISC-EB (orange) pairs. Increasingly darker orange lines correspond to the contact area distributions of ISC-EB pairs with size limits of the EB of the pair is as in E. Data in B-F are from a separate, larger dataset than that in A. **G**. Inset of the phase space (corresponding to the white square in Fig. 2A), with shaded boxes indicating the ranges of a and b values where the pair type frequencies from Fig. 1E (upper panel) and Fig. 1F (lower panel) best fit the model. For each experimental condition the height of the box is determined by the neighbourhood of b values where $H \leq 0.02$; the values of a determining the width of the box are obtained from Eqn. 7 using the best fitting value for c (when b equals the value at the mid-height of the box) and the SKD depicted in C to obtain experimentally supported values for A. Note the difference in scale between the two axes, evident even with the log-log scale. **H**. Fate outputs for the lateral inhibition model for different amounts of contact area.

703   The order of fate outcomes with increasing contact area follows the

704   experimental data in A.

Table 1. Cell-fate profiles as obtained experimentally ('data' column) and theoretically ('model' column). The values of b are those at the mid-height of the boxes in Fig. 4G corresponding to each of the genetic conditions in the table. The values of c are those with lowest value of Kullback-Leibler entropy H when b takes the value in the same row of this table.

dataset	condition	pair type	pair frequency		parameter value intervals		H
			data	model	b	c	
Figure 1E	$N^{+/+}$	ISC-ISC	4.7 %	5.1 %	0.26 ± 0.05	11	1.8×10^{-4}
		EB-EB	10.6 %	10.7 %			
		ISC-EB	84.7 %	84.2 %			
	$l(1)N^{B}/+$	ISC-ISC	0 %	0.7 %	0.15 ± 0.07	1.75	1.3×10^{-2}
		EB-EB	13.4 %	17.4 %			
		ISC-EB	86.6 %	81.9 %			
	$N^{55e11}/+$	ISC-ISC	12.2 %	11.7 %	0.20 ± 0.03	16	2.9×10^{-4}
		EB-EB	5.6 %	6.1 %			
		ISC-EB	82.2 %	82.2 %			
Figure 1F *da-GS, UAS-N^{RNAi}* (3 days with RU486)	mock	ISC-ISC	20.5 %	18.8 %	0.24 ± 0.03	23	1.5×10^{-3}
		EB-EB	22.7 %	24.6 %			
		ISC-EB	56.8 %	56.6 %			
	20μg	ISC-ISC	70.3 %	69.9 %	0.174 ± 0.004	49	3.9×10^{-4}
		EB-EB	3.7 %	4.2 %			
		ISC-EB	26.0 %	25.9 %			
	50μg	ISC-ISC	89.9 %	90.0 %	0.174 ± 0.004	64	1.6×10^{-2}
		EB-EB	1.0 %	3.4 %			
		ISC-EB	9.1 %	6.6 %			

References

Agrawal, S., Archer, C. and Schaffer, D. V. (2009). Computational Models of the Notch Network Elucidate Mechanisms of Context-dependent Signaling. *PLoS Comput Biol* **5**, e1000390–14.

Alcolea, M. P., Greulich, P., Wabik, A., Frede, J., Simons, B. D. and Jones, P. H. (2014). Differentiation imbalance in single oesophageal progenitor cells causes clonal immortalization and field change. *Nature Cell Biology* **16**, 615–622.

Arias, A. M. and Stewart, A. (2002). *Molecular Principles of Animal Development*. Oxford University Press, USA.

Artavanis-Tsakonas, S., Rand, M. D. and Lake, R. J. (1999). Notch signaling: cell fate control and signal integration in development. *science (New York, NY)* **284**, 770–776.

Baker, A.-M., Cereser, B., Melton, S., Fletcher, A. G., Rodriguez-Justo, M., Tadrous, P. J., Humphries, A., Elia, G., McDonald, S. A. C., Wright, N. A., et al. (2014). Quantification of crypt and stem cell evolution in the normal and neoplastic human colon. *CellReports* **8**, 940–947.

Bardin, A. J., Perdigoto, C. N., Southall, T. D., Brand, A. H. and Schweisguth, F. (2010). Transcriptional control of stem cell maintenance in the Drosophila intestine. *Development* **137**, 705–714.

Biteau, B., Hochmuth, C. E. and Jasper, H. (2008). JNK activity in somatic stem cells causes loss of tissue homeostasis in the aging Drosophila gut. *Cell Stem Cell* **3**, 442–455.

Boareto, M., Jolly, M. K., Lu, M., Onuchic, J. N., Clementi, C. and Ben-Jacob, E. (2015). Jagged–Delta asymmetry in Notch signaling can give rise to a Sender/Receiver hybrid phenotype. *Proceedings of the National Academy of Sciences* **112**, E402–E409.

Bray, S. and Furriols, M. (2001). Notch pathway: making sense of suppressor of hairless. *Curr Biol* **11**, R217–21.

Brennan, K., Tateson, R., Lewis, K. and Arias, A. M. (1997). A functional analysis of Notch mutations in Drosophila. *Genetics* **147**, 177–188.

Collier, J. R., Monk, N. A., Maini, P. K. and Lewis, J. H. (1996). Pattern formation by lateral inhibition with feedback: a mathematical model of delta-notch intercellular signalling. *J Theor Biol* **183**, 429–446.

de Back, W., Zhou, J. X. and Brusch, L. (2013). On the role of lateral stabilization during early patterning in the pancreas. *Journal of The Royal Society Interface* **10**, 20120766.

de Navascués, J., Perdigoto, C. N., Bian, Y., Schneider, M. H., Bardin, A. J., Martinez-Arias, A. and Simons, B. D. (2012). Drosophila midgut homeostasis involves neutral competition between symmetrically dividing intestinal stem cells. *EMBO J* **31**, 2473–2485.

Doupé, D. P., Alcolea, M. P., Roshan, A., Zhang, G., Klein, A. M., Simons, B. D. and Jones, P. H. (2012). A Single Progenitor Population Switches Behavior to Maintain and Repair Esophageal Epithelium. *science (New York, NY)* **337**, 1091–1093.

Dutta, D., Dobson, A. J., Houtz, P. L., Gläßer, C., Revah, J., Korzelius, J., Patel, P. H., Edgar, B. A. and Buchon, N. (2015). Regional Cell-Specific Transcriptome Mapping Reveals Regulatory Complexity in the Adult Drosophila Midgut. *CellReports* 1–14.

Ehebauer, M., Hayward, P. and Arias, A. M. (2006). Notch, a universal arbiter of cell fate decisions. *science (New York, NY)* **314**, 1414–1415.

Fang, H. Y., Martinez-Arias, A. and de Navascués, J. (2016). Autocrine and paracrine Wingless signalling in the Drosophila midgut by both continuous gradient and asynchronous bursts of wingless expression. *F1000Res* **5**, 317–14.

Formosa-Jordan, P., Ibanes, M., Ares, S. and Frade, J. M. (2012). Regulation of neuronal differentiation at the neurogenic wavefront. *Development* **139**, 2321–2329.

Friedmann, D. R. and Kovall, R. A. (2010). Thermodynamic and structural insights into CSL-DNA complexes. *Protein Science* **19**, 34–46.

Goulas, S., Conder, R. and Knoblich, J. A. (2012). The Par Complex and Integrins Direct Asymmetric Cell Division in Adult Intestinal Stem Cells. *Cell Stem Cell* **11**, 529–540.

Greenwald, I. (1998). LIN-12/Notch signaling: lessons from worms and flies. *Genes & Development* **12**, 1751–1762.

Guo, Z. and Ohlstein, B. (2015). Bidirectional Notch signaling regulates Drosophila intestinal stem cell multipotency. *science (New York, NY)* **350**, aab0988–aab0988.

Hsu, C.-P., Lee, P.-H., Chang, C.-W. and Lee, C.-T. (2006). Constructing quantitative models from qualitative mutant phenotypes: preferences in selecting sensory organ precursors. *Bioinformatics* **22**, 1375–1382.

Khait, I., Orsher, Y., Golan, O., Binshtok, U., Gordon-Bar, N., Amir- Zilberstein, L. and Sprinzak, D. (2015). Quantitative analysis of Delta-like-1 membrane dynamics elucidates the role of contact geometry on Notch signaling. *cell reports* **In Press**, 1–27.

Kidd, S., Lockett, T. J. and Young, M. W. (1983). The Notch locus of Drosophila melanogaster. *Cell* **34**, 421–433.

Kim, N.-G., Koh, E., Chen, X. and Gumbiner, B. M. (2011). E-cadherin mediates contact inhibition of proliferation through Hippo signaling-pathway components. *Proceedings of the National Academy of Sciences* **108**, 11930–11935.

Klein, A. M. and Simons, B. D. (2011). Universal patterns of stem cell fate in cycling adult tissues. *Development* **138**, 3103–3111.

792   **Koch, U., Lehal, R. and Radtke, F.** (2013). Stem cells living with a Notch.
793   *Development* **140**, 689–704.

794   **Krieger, T. and Simons, B. D.** (2015). Dynamic stem cell heterogeneity.
795   *Development* **142**, 1396–1406.

796   **Kullback, S. and Leibler, R. A.** (1951). On Information and Sufficiency. *Ann. Math.*
797   *Statist.* 79–86.

798   **LeVeque, R. J.** (2007). Finite difference methods for ordinary and partial differential
799   equations: steady-state and time-dependent problems (Vol. **98**). SIAM.

800   **Lyman, D. and Young, M. W.** (1993). Further evidence for function of the Drosophila
801   Notch protein as a transmembrane receptor. *Proc Natl Acad Sci USA* **90**, 10395–
802   10399.

803   **Maeda, K., Takemura, M., Umemori, M. and Adachi-Yamada, T.** (2008). E-
804   cadherin prolongs the moment for interaction between intestinal stem cell and its
805   progenitor cell to ensure Notch signaling in adult Drosophila midgut. *Genes Cells*
806   **13**, 1219–1227.

807   **Manders, E. M. M., Verbeek, F. J. and Aten, J. A.** (1993). Measurement of co-
808   localization of objects in dual-colour confocal images. *Journal of Microscopy* **169**,
809   375–382.

810   **Micchelli, C. A. and Perrimon, N.** (2006). Evidence that stem cells reside in the
811   adult Drosophila midgut epithelium. *Nature* **439**, 475–479.

812   **Miller, K. G., Field, C. M. and Alberts, B. M.** (1989). Actin-binding proteins from
813   Drosophila embryos: a complex network of interacting proteins detected by F-
814   actin affinity chromatography. *The Journal of Cell Biology* **109**, 2963–2975.

815   **Montagne, C. and González-Gaitán, M.** (2014). Sara endosomes and the
816   asymmetric division of intestinal stem cells. *Development* **141**, 2014–2023.

817   **Muñoz-Descalzo, S., Tkocz, K., Balayo, T. and Arias, A. M.** (2011). Modulation of
818   the ligand-independent traffic of Notch by Axin and Apc contributes to the
819   activation of Armadillo in Drosophila. *Development* **138**, 1501–1506.

820   **Nagarkar-Jaiswal, S., Lee, P. T., Campbell, M. E. and Chen, K.** (2015). A library of
821   MiMICs allows tagging of genes and reversible, spatial and temporal knockdown
822   of proteins in Drosophila. *eLife*.

823   **Ohlstein, B. and Spradling, A.** (2006). The adult Drosophila posterior midgut is
824   maintained by pluripotent stem cells. *Nature* **439**, 470–474.

825   **Ohlstein, B. and Spradling, A.** (2007). Multipotent Drosophila intestinal stem cells
826   specify daughter cell fates by differential notch signaling. *science (New York, NY)*
827   **315**, 988–992.

828   **Osterwalder, T., Yoon, K. S., White, B. H. and Keshishian, H.** (2001). A
829   conditional tissue-specific transgene expression system using inducible GAL4.
830   *Proc Natl Acad Sci USA* **98**, 12596–12601.

831 **Othmer, H. G. and Scriven, L. E.** (1971). Instability and dynamic pattern in cellular
832   networks. *J Theor Biol* **32**, 507–537.

833 **Pei, Z. and Baker, N. E.** (2008). Competition between Delta and the Abruptex
834   domain of Notch. *BMC Dev Biol* **8**, 4.

835 **Petrovic, J., Formosa-Jordan, P., Luna-Escalante, J. C., Abello, G., Ibanes, M.,**
836   **Neves, J. and Giraldez, F.** (2014). Ligand-dependent Notch signaling strength
837   orchestrates lateral induction and lateral inhibition in the developing inner ear.
838   *Development* **141**, 2313–2324.

839 **Plahte, E.** (2001). Pattern formation in discrete cell lattices. *J Math Biol* **43**, 411–445.

840 **Presente, A., Shaw, S., Nye, J. S. and Andres, A. J.** (2002). Transgene-mediated
841   RNA interference defines a novel role for notch in chemosensory startle
842   behavior. *Genesis* **34**, 165–169.

843 **Quiñones-Coello, A. T., Petrella, L. N., Ayers, K., Melillo, A., Mazzalupo, S.,**
844   **Hudson, A. M., Wang, S., Castiblanco, C., Buszczak, M., Hoskins, R. A., et**
845   **al.** (2007). Exploring strategies for protein trapping in Drosophila. *Genetics* **175**,
846   1089–1104.

847 **Rouault, H. and Hakim, V.** (2012). Different Cell Fates from Cell-Cell Interactions:
848   Core Architectures of Two-Cell Bistable Networks. *Biophysj* **102**, 417–426.

849 **Sanders, P. G. T., Muñoz-Descalzo, S., Balayo, T., Wirtz-Peitz, F., Hayward, P.**
850   **and Arias, A. M.** (2009). Ligand-independent traffic of Notch buffers activated
851   Armadillo in Drosophila. *PLoS Biol* **7**, e1000169.

852 **Schlegelmilch, K., Mohseni, M., Kirak, O., Pruszak, J., Rodriguez, J. R., Zhou,**
853   **D., Kreger, B. T., Vasioukhin, V., Avruch, J., Brummelkamp, T. R., et al.**
854   (2011). Yap1 acts downstream of α-catenin to control epidermal proliferation.
855   *Cell* **144**, 782–795.

856 **Shaya, O. and Sprinzak, D.** (2011). From Notch signaling to fine-grained patterning:
857   Modeling meets experiments. *Curr. Opin. Genet. Dev.* 1–8.

858 **Silvis, M. R., Kreger, B. T., Lien, W.-H., Klezovitch, O., Rudakova, G. M.,**
859   **Camargo, F. D., Lantz, D. M., Seykora, J. T. and Vasioukhin, V.** (2011). α-
860   catenin is a tumor suppressor that controls cell accumulation by regulating the
861   localization and activity of the transcriptional coactivator Yap1. *Science Signaling*
862   **4**, ra33–ra33.

863 **Simons, B. D. and Clevers, H.** (2011). Strategies for homeostatic stem cell self-
864   renewal in adult tissues. *Cell* **145**, 851–862.

865 **Simpson, P.** (2001). Notch signalling in development: on equivalence groups and
866   asymmetric developmental potential. *Curr. Opin. Genet. Dev.* **7**, 537–542.

867 **Spradling, A. C., Stern, D., Beaton, A. and Rhem, E. J.** (1999). The Berkeley
868   Drosophila Genome Project gene disruption project: Single P-element insertions
869   mutating 25% of vital Drosophila genes. *???*

870 **Sprinzak, D., Lakhanpal, A., LeBon, L., Garcia-Ojalvo, J. and Elowitz, M. B.**

871 (2011). Mutual Inactivation of Notch Receptors and Ligands Facilitates
872 Developmental Patterning. *PLoS Comput Biol* **7**, e1002069.

873 **Sprinzak, D., Lakhanpal, A., LeBon, L., Santat, L. A., Fontes, M. E., Anderson,**
874 **G. A., Garcia-Ojalvo, J. and Elowitz, M. B.** (2010). Cis-interactions between
875 Notch and Delta generate mutually exclusive signalling states. *Nature* **465**, 86–
876 90.

877 **Tepass, U. and Hartenstein, V.** (1994). The Development of Cellular Junctions in
878 the Drosophila Embryo. *Developmental Biology* **161**, 563–596.

879 **Tepass, U., Tanentzapf, G., Ward, R., & Fehon, R.** (2001). Epithelial cell polarity
880 and cell junctions in Drosophila. *Annual Review of Genetics* **35**, 747–784.

881 **Tricoire, H., Battisti, V., Trannoy, S., Lasbleiz, C., Pret, A.-M. and Monnier, V.**
882 (2009). The steroid hormone receptor EcR finely modulates Drosophila lifespan
883 during adulthood in a sex-specific manner. *Mech. Ageing Dev.* **130**, 547–552.

884 **Vermeulen, L., Morrissey, E., van der Heijden, M., Nicholson, A. M., Sottoriva,**
885 **A., Buczacki, S., Kemp, R., Tavaré, S. and Winton, D. J.** (2013). Defining stem
886 cell dynamics in models of intestinal tumor initiation. *science (New York, NY)*
887 **342**, 995–998.

888 **Zeng, X. and Hou, S. X.** (2015). Enteroendocrine cells are generated from stem cells
889 through a distinct progenitor in the adult Drosophila posterior midgut.
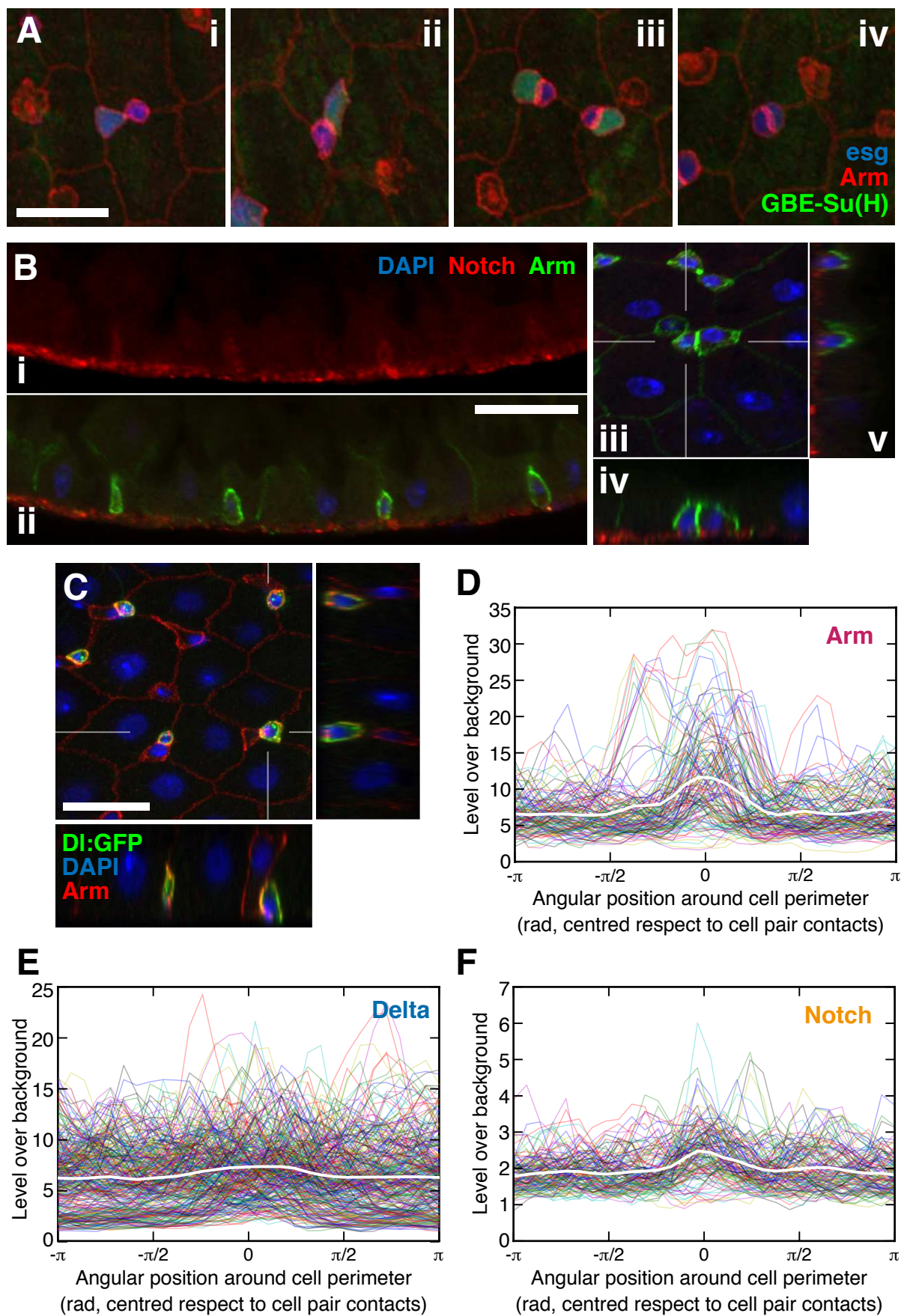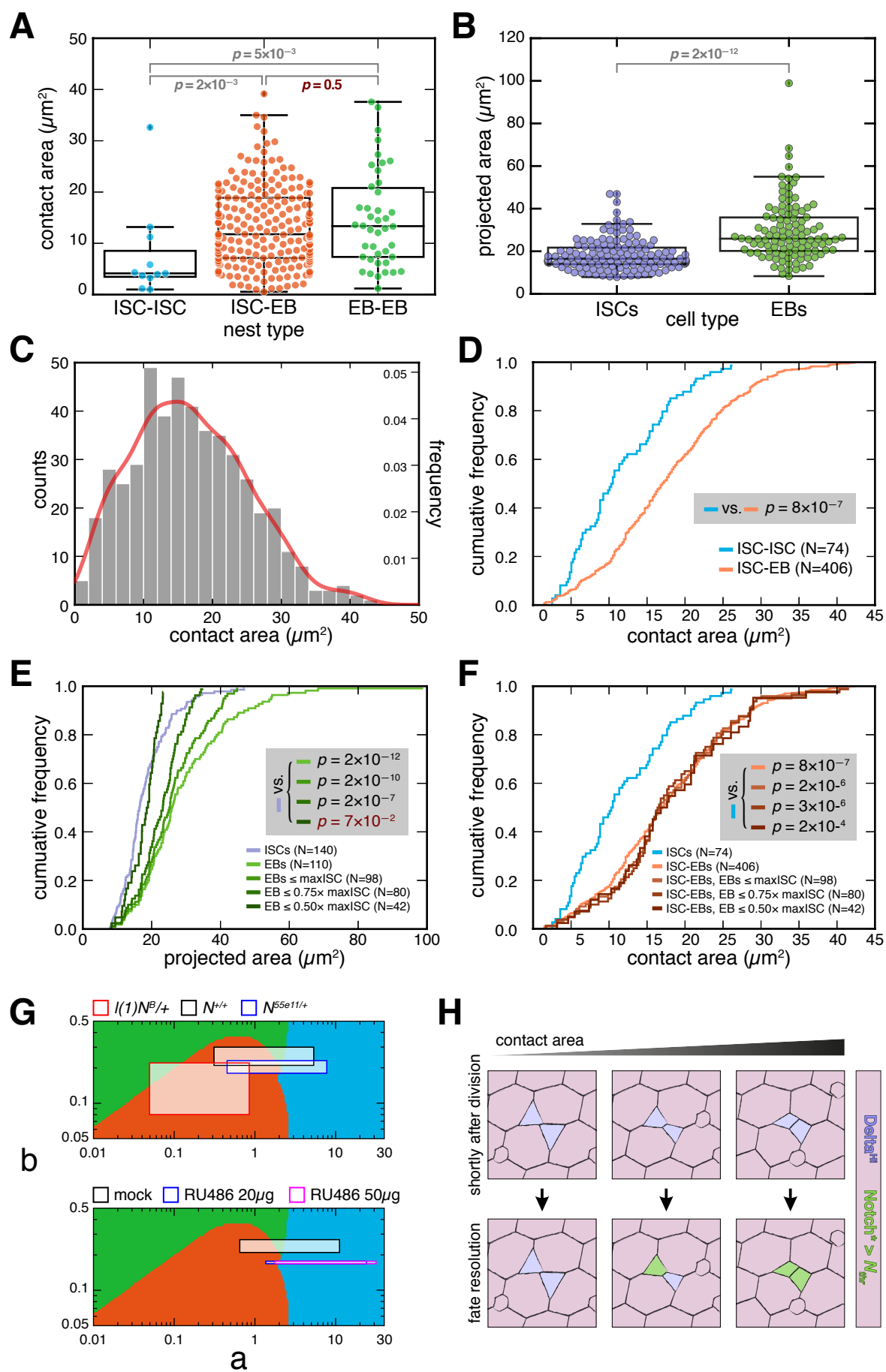890 *Development* **142**, 644–653.

891

892

Figure 1

A

esg
Arm/Pros
GBE-Su(H)

B

ISC — Delta⁺ esg⁺

EB — *Su(H)GBE⁺* esg⁺

EC

C   i   ii   iii

D

ISC-ISC
ISC-EB
EB-EB

E

Notch signalling

frequency

l(1)Nᴮ/+   *N⁺/⁺*   *N⁵⁵ᵉ¹¹/+*

G

Notch signalling

frequency

1.0
0.8
0.6
0.4
0.2
0.0

181 | 237   221 | 249   227 | 199

N¹¹ᴺ⁻ᴮ/+   *N⁺/⁺*   *N⁵⁵ᵉ¹¹/+*

EB
ISC

H

Notch signalling

frequency

1.0
0.8
0.6
0.4
0.2
0.0

751 | 653   912 | 202   613 | 48

mock   20   50
RU486 (μg/vial)

F

Notch signalling

frequency

0.8
0.6
0.4
0.2

mock   20   50
RU486 (μg/vial)
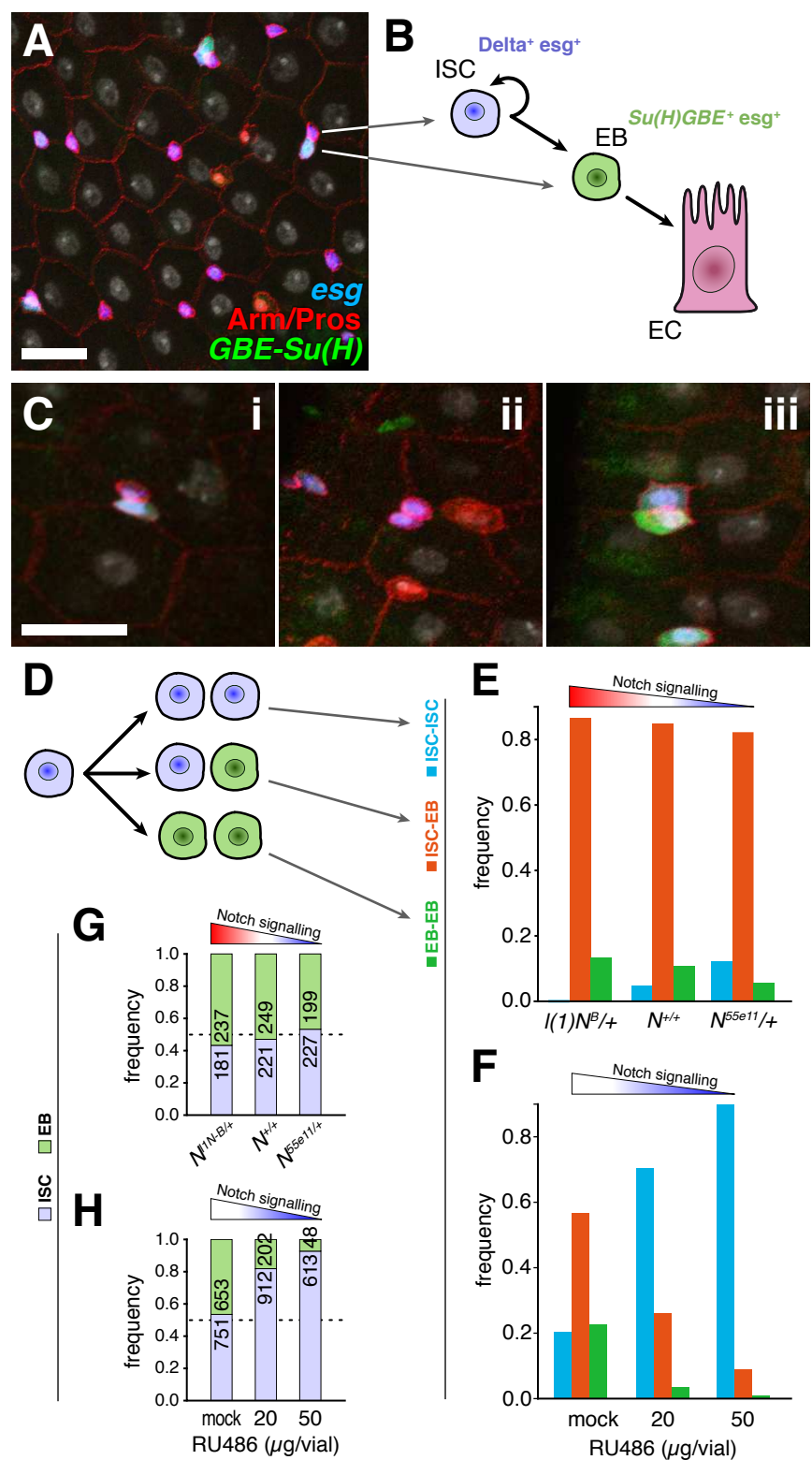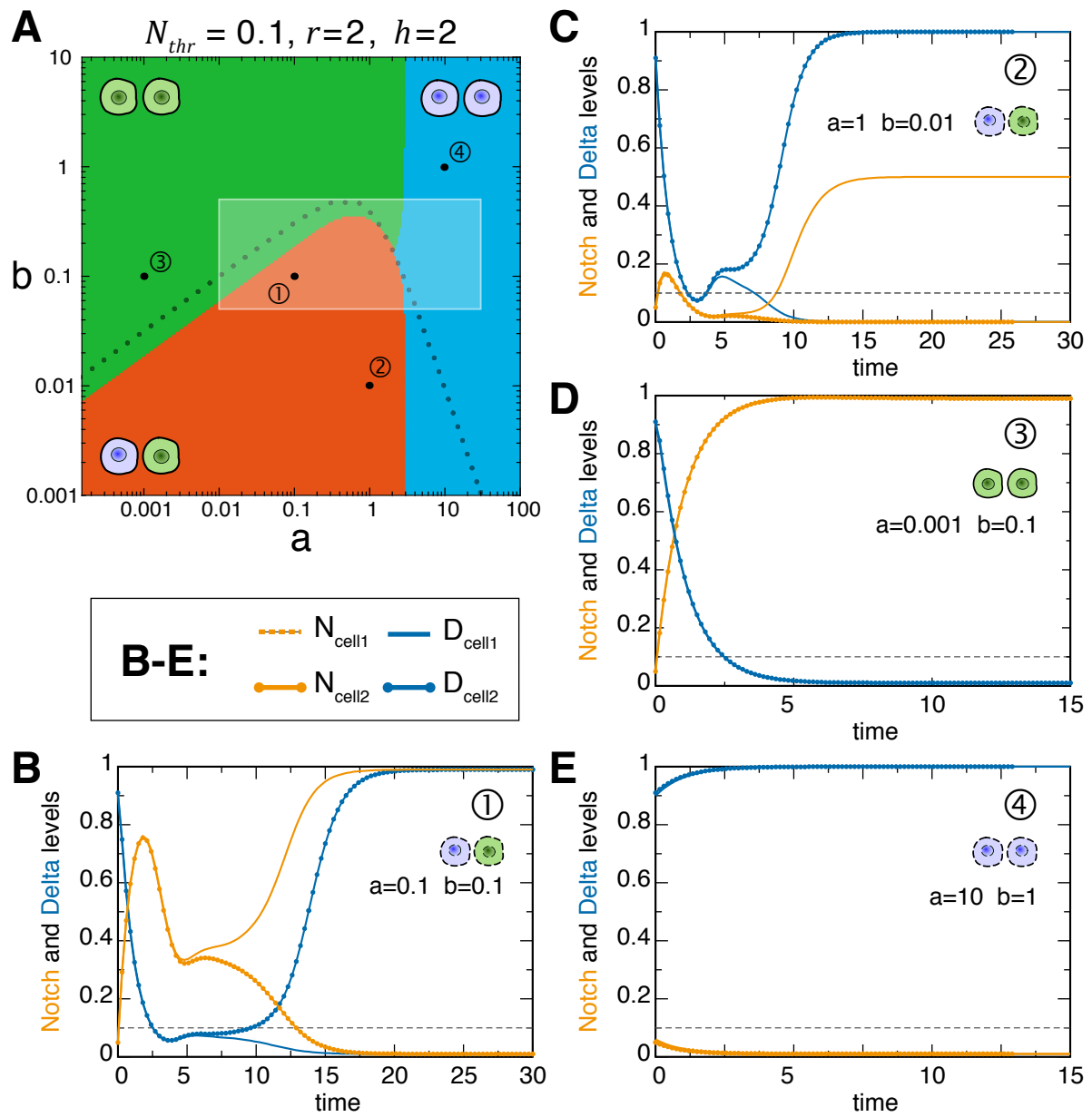
Figure 2

Figure 3

Figure 4

Supplementary Figure S1. The model behaviour is robust to variations in N_{thr} and cooperativity strength. **A**. Fate profiles in parameter space as in Fig. 2A, for comparison. **B-E**. Phase space for N_{thr} equal to 0.8 (B), 0.3 (C), 0.01 (D), and 0.001 (E), respectively (with $r, h = 2$ in all cases). The dotted line marks the stability boundary for the 'homogeneous' solutions (pairs of identical cells), and serves as reference for comparison with (A). While in B (where $N_{thr} > 0.7$), the area of asymmetric fate is surrounded by symmetric negative resolution, in C-E the organisation of the phase space is very similar to A, with the transitions shifting along the stability boundary. **F-H**. Phase space when cooperativity is either increased (in the repression of Dl by activated N, with $h = 5$, in F; or in the activation of N by Dl, with $r = 5$, in G) or eliminated (with $r, h = 1$, in H). ($N_{thr} = 0.1$ in all cases). Phase space in F, G is qualitatively similar to A, but not in H, where the asymmetric pairs are lost.

Supplementary Figure S2. *Notch* knock-down using *da-GS* is EB and ISC-specific and can induce a phenotypic series. **A**. Confocal micrograph showing the expression pattern of the *da-GS* driver, shown with *UAS-Stinger*. The same panel is repeated three times: left, with all markers (Stinger, green; Delta/Prospero, red; *GBE-Su(H)-lacZ*, blue; DNA, grey), center, with Stinger and *GBE-Su(H)-lacZ* (purple) only, and right, with Stinger and Delta/Prospero (purple) only. Delta accumulates at the membrane and vesicles; Prospero is nuclear. Note expression is highly specific of ISCs (Delta[+]) and EBs (*GBE-Su(H)-lacZ[+]*), only occasionally showing expression in EEs (Pros[+]; not shown). **B**. Cumulative frequency of nest size for *da-GS, UAS-N[RNAi]* flies with different RU486 treatments, with N = {956, 782, 394, 457} for mock, 20, 50 and 500μg/vial, respectively. Note the similarity in distributions between mock, 20 and 50μg/vial (with only the latter having a barely significant p-value), which breaks down evidently with 500μg/vial. **C-F.** Confocal micrographs showing esg[+] cell nests after mock treatment (C) and *Notch* knock-down induced with 20 (D), 50 (E) and 500μg/vial (F), respectively. ISC-like tumours are starting to form only with the 500μg/vial treatment.

31 **Supplementary Figure S3.** Values of Notch and Delta at steady state across
32 parameter space for $r = 2, h = 2$ (as in Figure 2A). Dotted line, boundary of
33 stability for steady states with identical cells. The black dots mark the
34 parameter values used in (Collier et al., 1996) (Figure 2B) and the
35 asymmetric, symmetric positive and symmetric negative pairs from Figure 2C-
36 E. **A, B.** Steady-state values of activated Notch in the two cells of a pair (one
37 in each panel) respect to a, b. **C-D.** Steady-state values of Delta in the two
38 cells of a pair (one in each panel) respect to a, b. Note that depending on the
39 value of activated Notch, one can find symmetric negative or symmetric
40 positive fate profiles below the boundary (region of heterogeneous solution),
41 showing that the model allows for symmetric steady states where cells in a
42 pair do not have identical amounts of Notch or Delta.

43 **Supplementary Figure S4.** Co-localisation between immunodetection of
44 Delta and GFP using $Delta^{MI04868\text{-}GFSTF.1}$. **A.** Confocal micrograph illustrating
45 the co-localisation of anti-Dl and anti-GFP in $Delta^{MI04868\text{-}GFSTF.1}/+$ intestines.
46 (Image shows the projection of several confocal planes). **B-C**. Co-localisation
47 measurements between anti-Dl, anti-GFP (for $Delta^{MI04868\text{-}GFSTF.1}$), anti-Arm as
48 a general membrane marker and Hoechst to label DNA, taken in 3D stacks for
49 individual cells. N indicates the number of cells measured per experiment.
50 Considering either Pearson correlation coefficient (B) or Manders
51 co-localisation coefficient (C), the data show a high level of co-localisation
52 between anti-Dl and anti-GFP, with very significantly higher coefficient values
53 than between anti-GFP and Hoechst (which would give the baseline values for
54 anti-correlation in this setting) as well as between anti-GFP and anti-Arm. The
55 latter comparison indicates that the level of correlation between anti-Dl and
56 anti-GFP cannot be from just coinciding randomly in the membrane and
57 demonstrates that, at this level of spatial resolution, detection of $Delta^{MI04868\text{-}}$
58 $^{GFSTF.1}$ with anti-GFP is a very good indicator of the spatial distribution of
59 Delta.

60 **Supplementary Figure S5.** Distribution of Arm, Notch and Delta at the
61 membrane. **A-C.** Histograms of the normalised mean intensity per plane (left

62   hand panels) and the coefficient of variation (CV) per plane (right hand

63   panels) for Arm (A), Notch (B) and Delta (C). The normalised mean intensity

64   in plane *i* is defined as the ratio of the average of the plane and the average

65   for the cell. Data correspond to 46 cells (single and paired) for Notch and

66   Armadillo, and 66 cells (paired) for Delta. **D-F**. Distribution of Arm (D), Notch

67   (E) and Dl (F) levels along the apical-basal cell axis (with height of the cell

68   normalised to 1). Each cell contributes ten lines to the plot, corresponding to

69   the intensity values along the vertical axis of non-overlapping, angular

70   windows of $2\pi/10$. Data displayed in D-E are from 20 paired esg+ cells and

71   data in F are from 43 cells.

72   **Supplementary Figure S6.** Relationships between cell size, Arm levels and

73   contact area, and statistical comparison between theoretical and experimental

74   pair frequencies. Data in A-D are from the cell set from Figure 4B. **A**.

75   Correlation between cell volume and projected cell area for EBs and ISCs,

76   showing that projected area is a good predictor of total volume. **B**.

77   Comparison of volume between ISCs and EBs. EBs are ~60% larger, with

78   statistical significance. **C**. Correlation between contact area and projected cell

79   area of the cells in the pair. The larger cells in each pair (usually an EB) is

80   represented in dark blue and the smaller (usually an ISC) in light brown. **D**.

81   Correlation between cell volume and projected cell area of the cells in the pair.

82   Colour scheme is as in C. **E-F**. Arm levels along the perimeter of ISCs in

83   either ISC-ISC (E) or ISC-EB (F) pairs, for all cells confocal planes (colour

84   lines), with the mean value (white). For each cell plane, position 0

85   corresponds to the centre of the contacting membranes (defined as the

86   position that intersects the line connecting the cell centroids in that plane).

87   Data in E-F are from 20 ISC-EB and 23 ISC-ISC pairs. **G-H**. Kullback-Leibler

88   relative entropy (*H*) between experimental and model distributions of *Notch*

89   wild-type (G) or mock *Notch* knockdown (H) cell pair frequencies as a function

90   of *b* and *c* (note the difference in scale between the two parameters). Values

91   of area in the model are generated by the SKD depicted in Fig. 4C. Best fits

92   (black dots) correspond to *b* = 0.26, *c* = 11 (G) and *b* = 0.24, *c* = 23 (H). Black

93   discontinuous lines mark isovalues every 0.05 H units. White discontinuous

94   lines enclose the area for $H \leq 0.02$; the upper and lower limits of b in these

95   areas define the height of the boxes in the parameter space indicated in Fig.
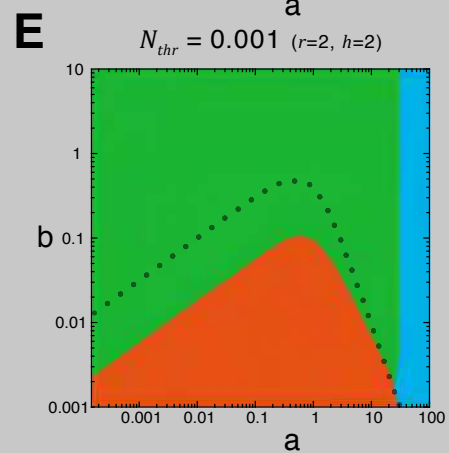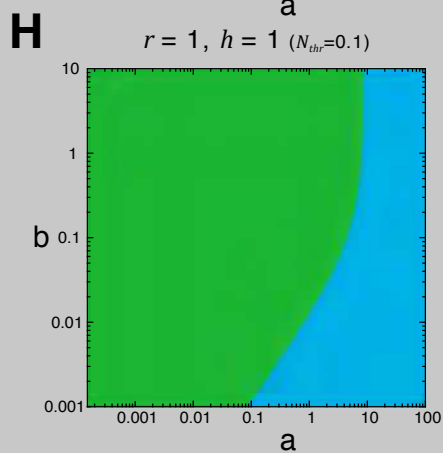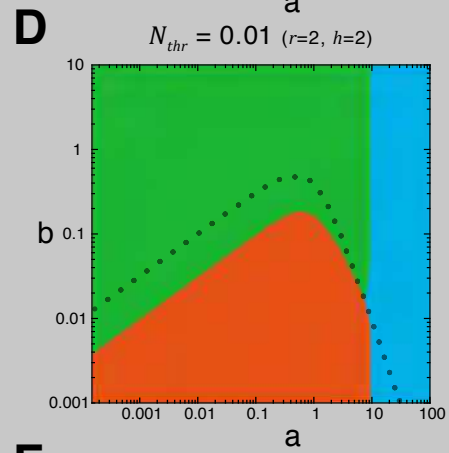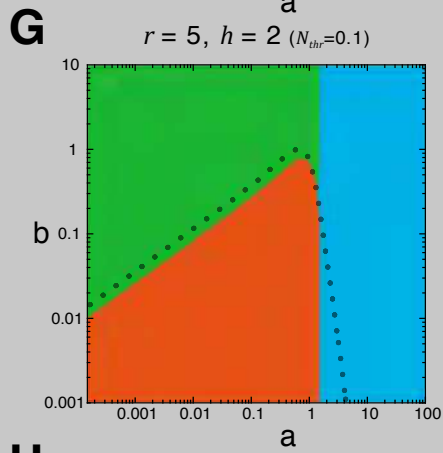
96   4G.

Supplementary Figure S1

A $N_{thr} = 0.1$, $r=2$, $h=2$
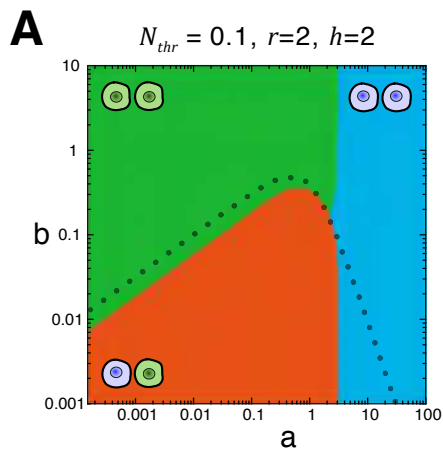
influence of N_{thr} in parameter space

B $N_{thr} = 0.8$ ($r=2$, $h=2$)
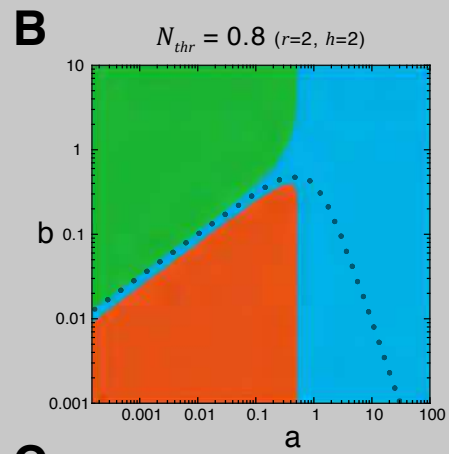
influence of **cooperativity** (r, h) in parameter space

F $r = 2$, $h = 5$ ($N_{thr}=0.1$)

C $N_{thr} = 0.3$ ($r=2$, $h=2$)

G $r = 5$, $h = 2$ ($N_{thr}=0.1$)

D $N_{thr} = 0.01$ ($r=2$, $h=2$)

H $r = 1$, $h = 1$ ($N_{thr}=0.1$)

E $N_{thr} = 0.001$ ($r=2$, $h=2$)

Supplementary Figure S2

da-GS, UAS-Stinger (3 days with RU486, 500μg)

A

DNA
Dl/Pros
GBE-Su(H)
StingerGFP

GBE-Su(H)

Dl/Pros

B

da-GS, UAS-N^{RNAi}, 3 days with RU486

cumulative frequency vs. cluster size

vs. { $p = 0.38$; $p = 0.06$; $p = 0.02$ }

mock
20μg
50μg
500μg

da-GS, UAS-N^{RNAi} (3 days with RU486)

C mock
esg
DNA
Arm/Pros
GBE-Su(H)

D RU486 20μg
esg
DNA
Arm/Pros
GBE-Su(H)

E RU486 50μg
esg
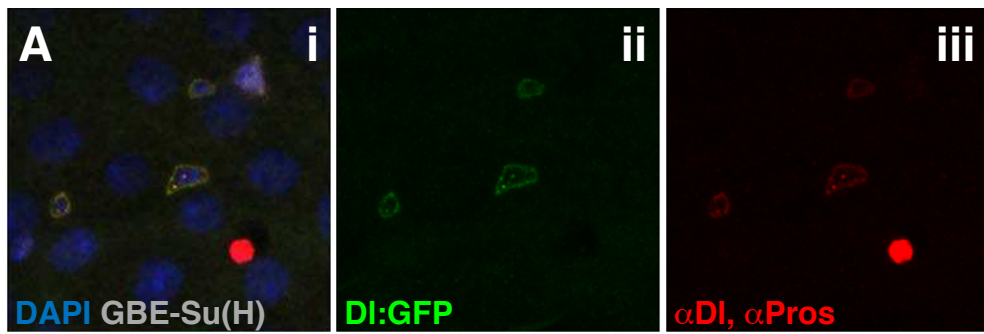DNA
Arm/Pros
GBE-Su(H)

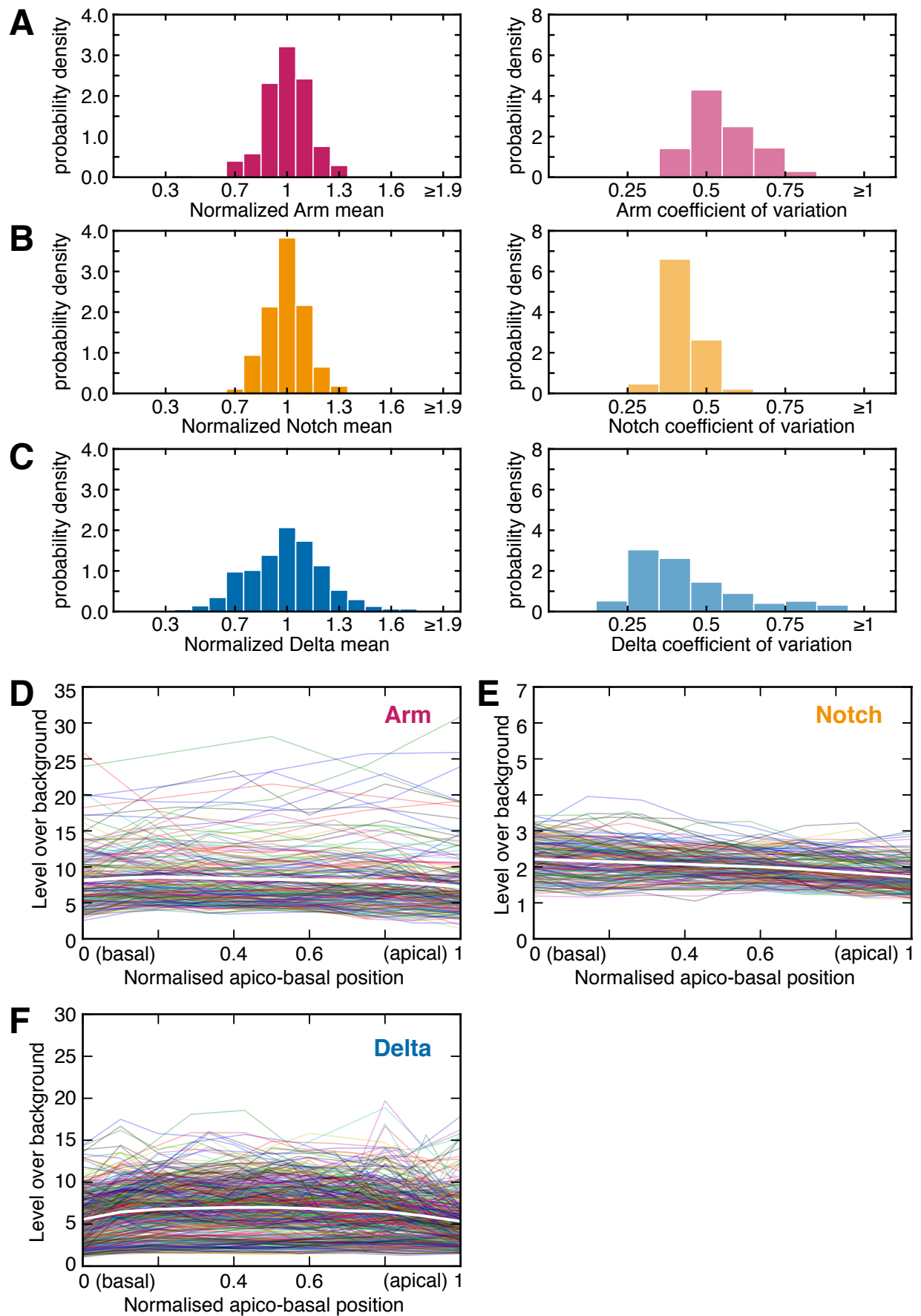**F** RU486 500μg
Dl
DNA
Arm:GFP

Supplementary Figure S3

Supplementary Figure S4
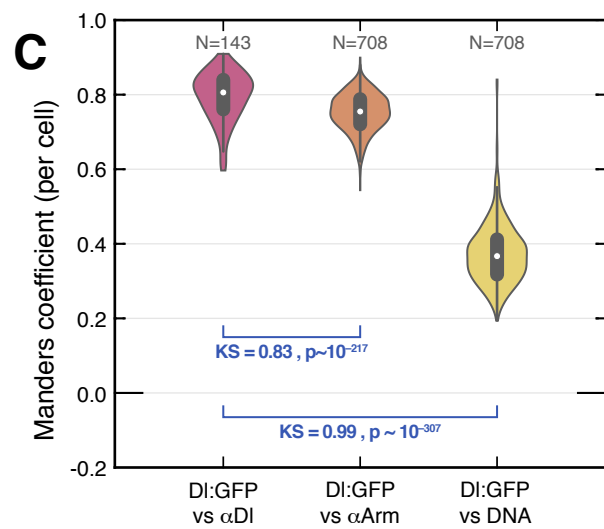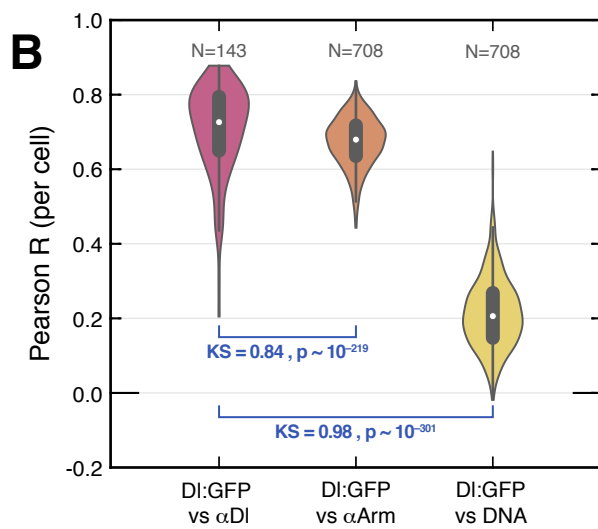
Supplementary Figure S5

Supplementary Figure S6